LASER SYSTEMS FOR APPLICATIONS

Edited by **Krzysztof Jakubczak**

INTECHWEB.ORG

Laser Systems for Applications
Edited by Krzysztof Jakubczak

Published by InTech
Janeza Trdine 9, 51000 Rijeka, Croatia

Publishing Process Manager Petra Nenadic
Technical Editor Teodora Smiljanic
Cover Designer InTech Design Team
Image Copyright pixomar, 2011.

First published December, 2011
Printed in Croatia

A free online edition of this book is available at www.intechopen.com
Additional hard copies can be obtained from orders@intechweb.org

Laser Systems for Applications, Edited by Krzysztof Jakubczak
p. cm.
ISBN 978-953-307-429-0

Contents

8

Controlling the Carrier-Envelope Phase of Few-Cycle Laser Beams in Dispersive Media

Carlos J. Zapata-Rodríguez[1] and Juan J. Miret[2]

[1]*Departament of Optics, University of Valencia, Burjassot*
[2]*Departament of Optics, Pharmacology and Anatomy, University of Alicante, Alicante*
Spain

1. Introduction

During the last decade it has been practicable to achieve a full control of the temporal evolution of the wave field of ultrashort mode-locked laser beams (1). Advances in femtosecond laser technology and nonlinear optics have made possible to tailor the phase and magnitude of the electric field leading to a wide range of new applications in science. Many physical phenomena are dependent directly on the electric field rather than the pulse envelope such as electron emission from ionized atoms (2) and metal surfaces (3), or carrier-wave Rabi-flopping (4). Moreover, attosecond physics is for all practical purposes accessible by using femtosecond pulses with controlled carrier-envelope (CE) phase conducting to coherent light generation in the XUV spectral regions (5). Additional applications in the frequency domain includes optical metrology where the laser spectrum is employed (6).

In this chapter we apply fundamental concepts of three-dimensional wave packets to illustrate not only transverse but what is more fascinating on-axis effects on the propagation of few-cycle laser pulses (7). The frequency-dependent nature of diffraction behaves as a sort of dispersion that makes changes in the pulse front surface, its group velocity, the envelope form, and the carrier frequency. The procedure lays on pulsed Gaussian beams, in which these changes are straightforwardly quantified. In particular, the carrier phase at any point of space near the beam axis is evaluated. Anomalous pulse front behavior including superluminality in pulsed Gaussian beams is also found. Finally the CE phase is computed in the focal volume and in the far field.

Generally focused pulses manifest a strong phase dispersion in the neighborhood of the geometrical focus, so that enhanced spatial resolution is achieved in CE phase-dependent phenomena. In some circumstances, however, increased depth of focus may be of convenience so that a stationary CE phase should be required in the near field. It is noteworthy that Gouy wave modes (8) show some control over on-axis phases demonstrating undistorted pulse focalization even in dispersive media. Practical realizations may be driven by angular dispersion engineering of ultrashort laser beams. In this concern we introduced the concept of dispersive imaging (9) as a tool for controlling the dispersive nature of broadband wave fields. Achromatic (10) and apochromatic (11) corrections of the angular spectrum of diffracted wave fields may be achieved with the use of highly-dispersive lenses such as kinoform-type zone plates. This procedure has been employed previously to compensate the longitudinal

chromatic aberration (12; 13) and also the diffraction-induced chromatic mismatching of Fraunhofer patterns (14; 15).
We exploit dispersive imaging assisted by zone plates to gain control over the waveforms of focused laser beams drawing near to Gouy waves modes. The theoretical analysis is addressed only to pulsed Gaussian beams for simplicity. We carry to term a lens system design applying the $ABCD$ matrix formalism. Fundamental attributes of a dispersive beam expander are provided in order to adjust conveniently the spatial dispersion of the collimated input beam. Numerical simulations evidence CE-phase stationarity of few-cycle focused pulses in dispersive media along the optical axis near the focus.

2. Carrier-envelope phase

Let us review in this section the basic grounds on linear wave propagation of few-cycle plane waves in dispersive media. In particular we consider the effect of the CE phase on the spectrum of a pulse train as it is launched by a mode-locked laser. Besides this sequel, nonlinear effects also give rise to a relative phase shift between carrier and envelope which are briefly discussed.

2.1 Pulsed plane waves

We start by considering a plane wave propagating in the z direction. Then we write the electric field amplitude at $z = 0$ as (16)

$$E(0,t) = \mathrm{Re} \int_{-\infty}^{\infty} S(\omega) \exp(-i\omega t) d\omega \tag{1}$$

The effect of propagation over a distance z is to multiply each Fourier component in the time domain by a factor $\exp(ikz)$. Note that the wavenumber varies upon the frequency as $k(\omega) = \omega n(\omega)/c$, where n is the index of refraction of the medium. Therefore we may write

$$E(z,t) = \mathrm{Re}\ E_0(z,t) \exp\left(ik_0 z - i\omega_0 t + i\varphi_0\right) \tag{2}$$

We are assuming a carrier wave with frequency and wavenumber ω_0 and $k_0 = k(\omega_0)$, respectively. Additionally, there is an envelope of the wave field that we denote by

$$E_0(z,t) = \int_{-\infty}^{\infty} S(\omega) \exp\left\{i[k(\omega) - k_0]z - i(\omega - \omega_0)t - i\varphi_0\right\} d\omega \tag{3}$$

The absolute phase $\varphi_0 = \arg \int S(\omega) d\omega$ represents the argument of the complex wave field at $z = 0$ and $t = 0$, leading to a real valued envelope E_0 at the origin.
The Taylor expansion of $k(\omega)$ around the carrier frequency,

$$k(\omega_0 + \Omega) = k_0 + \left(\frac{\partial k}{\partial \omega}\right)_{\omega_0} \Omega + \frac{1}{2}\left(\frac{\partial^2 k}{\partial \omega^2}\right)_{\omega_0} \Omega^2 + \ldots \tag{4}$$

where $\Omega = \omega - \omega_0$, gives

$$\frac{\partial E_0}{\partial z} + \dot{k}_0 \frac{\partial E_0}{\partial t} + \frac{i\ddot{k}_0}{2} \frac{\partial^2 E_0}{\partial t^2} + \ldots = 0. \tag{5}$$

From here on out we assume that a dot over a parameter stands for a derivative with respect to ω, and a subscript 0 denotes its evaluation at the specific frequency $\omega = \omega_0$. Therefore the

inverse velocity $\dot{k}_0$ represents $\partial_\omega k$ computed at $\Omega = 0$. This is also consistent with the fact that the carrier wavenumber k_0 symbolizes $k(\omega_0)$. It oftentimes comes to happen that $\ddot{k}_0 \partial_t^2 E_0$ and all the higher-derivative terms in (5) are negligible compared with the first-derivative terms. As a consequence Eq. (5) approaches

$$\frac{\partial E_0}{\partial z} + \frac{1}{v_g}\frac{\partial E_0}{\partial t} = 0. \tag{6}$$

The group velocity

$$v_g = \frac{1}{\dot{k}_0} = \frac{c}{n_0 + \omega_0 \dot{n}_0}, \tag{7}$$

where n_0 represents the real part of the refractive index, and c denotes the speed of light in vacuum. We point out that a negligible absorption at ω_0 is taken for granted, concluding that $\dot{k}_0$ may be set as purely real. In this approximation, the evolution of the the electric field is simply

$$E(z,t) = \mathrm{Re}\, E_0(0, t - z/v_g) \exp\left[-i\omega_0(t - z/v_p) + i\varphi_0\right] \tag{8}$$

Accordingly the pulse envelope propagates without change of shape or amplitude at the group velocity v_g. However, the phase of the field evolves with a velocity $v_p = \omega_0/k_0 = c/n_0$. In dispersive media, the group velocity and the phase velocity are clearly dissimilar. If otherwise we neglect dispersion by setting $\dot{n}_0 = 0$, it is finally inferred from (7) that both velocities coindice.

2.2 Few-cycle wave fields

For a short pulse of a duration much longer than an optical cycle, its envelope E_0 provides efficiently the time evolution of the wave field that is necessary to include in the vast majority of time-resolved electromagnetic phenomena. If, however, the pulse length is of the order of a single cycle, the phase variation of the wave becomes relevant upon the appropriate description of the electric field. The issue of the absolute phase of few-cycle light pulses was first addressed by Xu et al. (17). Their experiments revealed that the position of the carrier relative to the envelope is generally rapidly varying in the pulse train emitted from a mode-locked laser oscillator.

To understand the origin of this carrier phase shift, it is convenient to introduce a coordinate system that is moving with the pulse at the group velocity. Thus we follow the pulse evolution in this system. For that purpose we perform the coordinate transformation $t' = t - z/v_g$ and $z' = z$. Equation (8) in this moving frame of reference can then be rewritten as

$$E(z',t') = \mathrm{Re}\, E_0(0,t') \exp\left[-i\omega_0 t' + i\varphi(z')\right] \tag{9}$$

where the phase

$$\varphi(z') = \varphi_0 + \omega_0\left(\frac{1}{v_p} - \frac{1}{v_g}\right)z' = \varphi_0 - \frac{\omega_0^2 \dot{n}_0}{c} z'. \tag{10}$$

Note that $\varphi(z')$ determines the position of the carrier relative to the envelope.

In Fig. 1 we represent the pulse evolution in the time domain at different planes z' of an ultrashort wave field propagating in sapphire. The numerical simulations make use of a bandlimited signal $S(\Omega') = 1 - 2\Omega'^2 + \Omega'^4$ for $|\Omega'| < 1$, where $\Omega' = (\omega - \omega_0)/\Delta_0$. The mean frequency is $\omega_0 = 3.14$ fs^{-1} and the width of the spectral window is $0.8\omega_0$, i.e. $\Delta_0 = 0.4\omega_0$, providing a 4.8 fs (FWHM) transform-limited optical pulse. By inspecting $\varphi(z')$

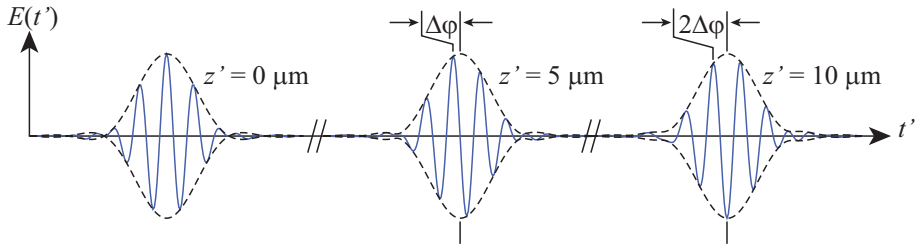

Fig. 1. Plane wave propagation in sapphire. The velocities $v_p = 0.566\ c$ and $v_g = 0.556\ c$ are estimated for a wavelength $\lambda_0 = 600$ nm in vacuum. The envelope is shown in dashed line.

we can identify the difference between the phase delay z'/v_p and the group delay z'/v_g as the reason that the carrier slides under the envelope as the pulse propagates in the dispersive medium. With regard to this matter it is common to introduce the dephasing length L_d as the propagation length over which the carrier is offset by a phase of π with respect to the envelope. Since we express the change in the carrier phase shift upon passage through a medium of length L as $\Delta\varphi = -\left(\omega_0^2 \dot{n}_0/c\right) L$, we finally obtain

$$L_d = \frac{\pi c/\omega_0^2}{|\dot{n}_0|} = \frac{1}{2}\left|\frac{\partial n}{\partial \lambda}\right|_{\lambda_0}^{-1}. \tag{11}$$

In Eq. (11), λ_0 represents the carrier wavelength as measured in vacuum. The dephasing length can be as short as 10 μm in sapphire, as illustrated in Fig. 1. Now it becomes obvious that the difference between phase and group delay in transparent optical materials originates from the wavelength dependence of the (real) refractive index.

2.3 Pulse train spectrum in a mode-locked laser

Considering a single pulse, for instance at $z = 0$, it will have an amplitude spectrum $S(\omega)$ that is centered at the optical frequency ω_0 of its carrier. From a mode-lock laser, however, we would obtain a train of pulses separated by a fixed interval $T = L_c/v_g$,

$$F(t) = \sum_m E(mL_c, t), \tag{12}$$

where L_c is the round-trip length of the laser cavity. For this case, the spectrum can easily be obtained by a Fourier series expansion,

$$\tilde{F}(\omega) = S(\omega)\sum_m \exp\left[im\Delta\varphi(L_c) - im\omega T\right] = S(\omega)\frac{2\pi}{T}\sum_m \delta\left(\omega - m\omega_r - \omega_{CE}\right). \tag{13}$$

This gives a comb of regularly spaced frequencies, where the comb spacing $\omega_r = 2\pi/T$ is inversely proportional to the time between pulses (18). Additionally we have considered that the CE phase is evolving with space, such that from pulse to pulse emitted by a mode-locked laser there is a phase increment of $\Delta\varphi(L_c) = \varphi(L_c) - \varphi_0$. Therefore, the carrier-wave is different for successive pulses and repeats itself with the frequency

$$\omega_{CE} = \frac{\Delta\varphi(L_c)}{2\pi}\omega_r, \tag{14}$$

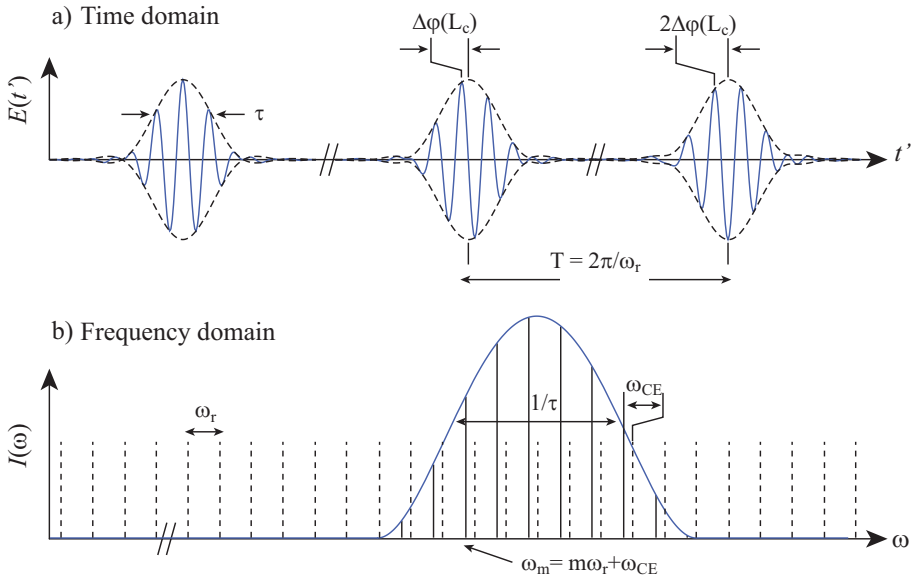

Fig. 2. Illustration of the time-frequency correspondence for a pulse train with evolving carrier-envelope phase.

that is called the carrier-envelope frequency (19). Then in the spectral domain, a rigid shift $\omega_{CE} = \Delta\varphi(L_c)/T$ will occur for the frequencies of the comb lines, as shown in Figure 2. Changing the linear or nonlinear contributions to the round-trip phase shift $\Delta\varphi(L_c)$ inside the laser cavity changes the CE frequency.

2.4 Nonlinear effects

In mode-locked lasers, nonlinear effects also give rise to a relative phase shift between the carrier and the envelope. This is not surprising as there is a nonlinear contribution to the phase shift of the intracavity pulse as it passes through the gain crystal. The most remarkable effect in femtosecond lasers is the third order Kerr nonlinearity responsible for self-phase modulation, which produces a significant spectral broadening. The Kerr effect leads to a self-phase shift of the carrier, similar to the soliton self-phase shift in fiber optics (20). The Kerr effect also induces a distortion of the envelope called self-steepening causing a group delay of the envelope with respect to the underlying carrier.

One of the first experiments to measure carrier-envelope phase evolution observed its intensity dependence (17). Further experiments showed that for shorter pulses, $\Delta\varphi$ was much less sensitive to changes in the pulse intensity (21). In order to give a response to this effect we may consider that the group velocity also depends on intensity. In fact the group velocity changes twice as fast with intensity as does the phase velocity (20). Novel theoretical treatment considered also the fact that dispersion and nonlinearity in the laser are not constant as a function of position in the cavity (22). At this stage, a number of phenomena have been identified in theory and experiment, although some aspects of the connection between them remain unclear.

We point out that the intensity dependence of the CE phase provides a parameter by which the carrier-envelope phase can be controlled. However, it means that the amplitude noise will be converted to phase noise.

3. CE phase of Gaussian laser beams

Since many lasers produce output beams in which the transverse intensity distribution is approximately Gaussian, there has been an appreciable interest in studying the properties of Gaussian beams. The exact Gaussian-like solution to the paraxial wave equation is introduced in this section. Thereafter we obtain analytical expressions of the Gouy phase shift and the CE phase shift of Gaussian beams. Finally we demonstrate that CE phase stationarity, i.e. conservation of the CE phase along with the z coordinate, requires a given spatial dispersion of the wave field to balance dispersion of the dielectric host medium.

3.1 The Gouy phase shift

The so-called Gouy phase is the subject of continuous investigation (23–26) since in 1890 Louis G. Gouy published a celebrated paper (27) on the longitudinal phase delay of spherical beams. Its relevance is a great deal more than purely academic. For instance, the superluminal phase velocity found in the focal region of paraxial Gaussian beams may be understood in terms of this phase anomaly (7). More recently, direct observation of Gouy phases has attracted the interest in the framework of single-cycle focused beams (28–32). In this context, the Gouy phase shift results of great importance for a wide variety of phenomena and applications involving high field physics and extreme nonlinear optics.

It is shown that an exact solution to the paraxial wave equation

$$\frac{\partial^2 \psi}{\partial x^2} + \frac{\partial^2 \psi}{\partial y^2} + 2ik(\omega)\frac{\partial \psi}{\partial z} = 0, \tag{15}$$

for a monochromatic beam of Gaussian cross section traveling in the $+z$ direction and centered on the z axis is given by (33)

$$\psi(\vec{R},\omega) = S(\omega)\frac{z_R}{iq(z,\omega)}\exp\left[ik(\omega)\frac{x^2+y^2}{2q(z,\omega)}\right] \tag{16}$$

where $\vec{R} = (x,y,z)$, (x,y being Cartesian coordinates in a plane perpendicular to the beam axis), $S(\omega) = \psi(\vec{0},\omega)$ is the in-focus time-domain spectrum of the field, and $q(z,\omega) = z - iz_R(\omega)$ stands for the complex radius of curvature. The parameter $z_R(\omega) = k(\omega)s^2/2$ is called the Rayleigh range, which depends on the spot size s at the beam waist. In fact, this term is commonly used to describe the distance that a collimated beam propagates from its waist ($z = 0$) before it begins to diverge significantly.

The monochromatic wave field of a Gaussian beam is completely described by including the phase-only term $\exp(ikz - i\omega t)$. In the vicinity of the beam axis, $(x,y) = (0,0)$, the phase front is approximately flat and the Gaussian beam behaves essentially like a plane wave. However, the evolution of the phase front along with the propagation distance z ceases to be linear. In particular, the phase shift of the complex wave field stored at different transverse planes from the beam waist is $\phi = kz - \phi_G$, where

$$\phi_G(z) = \arctan\left(\frac{z}{z_R}\right) \tag{17}$$

is the Gouy phase. Therefore, the wave accumulates a whole phase of π rads derived from the term ϕ_G, which is produced for the most part near the beam waist.
Let us provide an intuitive explanation of the physical origin of the Gouy phase shift, which is based on the transverse spatial confinement of the Gaussian laser beam. Through the uncertainty principle, localization of the wave field introduces a spread in the transverse momenta and hence a shift in the expectation value of the axial propagation constant (25). At this stage we consider a smooth variation of ϕ_G along the optical axis, which allows us to substitute ϕ by its first-order series expansion $[k - \partial_z \phi_G(z_0)]\, z - \phi_G(z_0) + z_0 \partial_z \phi_G(z_0)$ in the neighborhood of a given point z_0. Within a short interval around z_0, the wave front propagates with a spatial frequency $k - \partial_z \phi_G(z_0)$. Accordingly we conveniently introduce the local wavenumber $k_z(z, \omega) = \partial_z \phi$. For a Gaussian beam, the local wavenumber is simply

$$k_z = k - \frac{z_R}{z^2 + z_R^2}. \tag{18}$$

Note that k_z approaches the wavenumber k associated with a plane wave in the limit $z \to \pm\infty$. In the near field, however, k_z is lower than k and it reaches a minimum value at the beam waist.

3.2 The CE phase shift

We will show that the Gouy phase dispersion is determinant in the waveform of broadband optical pulses (7). This is commonly parametrized by the CE phase. For that purpose, let us consider a pulsed Gaussian beam once again. As mentioned above, the electromagnetic field near the beam axis evolves like a plane wave whose wave number k_z given in (18) will change locally. In this context, the temporal evolution of the wave field is fundamentally given by Eq. (9). This is a particularly accurate statement within the Rayleigh range of highly-confined Gaussian beams, which is based on the short-path propagation in the region of interest.
For non-uniform beams, the on-axis pulse propagation evolves at a local phase velocity $v_p(z) = \omega_0 / k_{z0}$ and group velocity $v_g(z) = \dot{k}_{z0}^{-1}$. Particularly, the phase velocity of the Gaussian beam in terms of the normalized axial coordinate $\zeta = z / z_{R0}$ is

$$v_p = c \left[n_{p0} - \frac{1}{\mathcal{L}_0 \left(1 + \zeta^2\right)} \right]^{-1}, \tag{19}$$

where z_{R0} is the Rayleigh range at the carrier frequency ω_0, and the Gaussian length $\mathcal{L} = k z_R / n$. Note that $\mathcal{L}_0 = k_0^2 s_0^2 / 2 n_{p0}$ also gives the area (which is conveniently normalized) of the beam waist at ω_0. On the other hand, the group velocity yields

$$v_g = c \left[n_{g0} + \frac{\mathcal{F}_0 \left(1 - \zeta^2\right)}{\mathcal{L}_0 \left(1 + \zeta^2\right)^2} \right]^{-1}, \tag{20}$$

where $n_g = c\dot{k}$ is the group index, and $\mathcal{F} = \omega \dot{z}_R / z_R$. In order to understand the significance of $\mathcal{F}$, let us conceive a Gaussian beam exhibiting an invariant $\mathcal{F}$ within a given spectral band around ω_0. This case would consider a dispersive Rayleigh range of the form $z_R = z_{R0} \left(\omega / \omega_0\right)^{\mathcal{F}}$, a model employed elsewhere (32). Therefore, $\mathcal{F}$ parametrizes the longitudinal dispersion of the Gaussian beam. This can be deduced also from the relationship $\mathcal{F} = \omega \dot{\mathcal{L}} / \mathcal{L} - 1$.
In Fig. 3(a) we compare graphically the phase velocity and the group velocity of pulsed Gaussian beams with $\mathcal{L}_0 = 34$ and different values of the parameter $\mathcal{F}_0$, which are

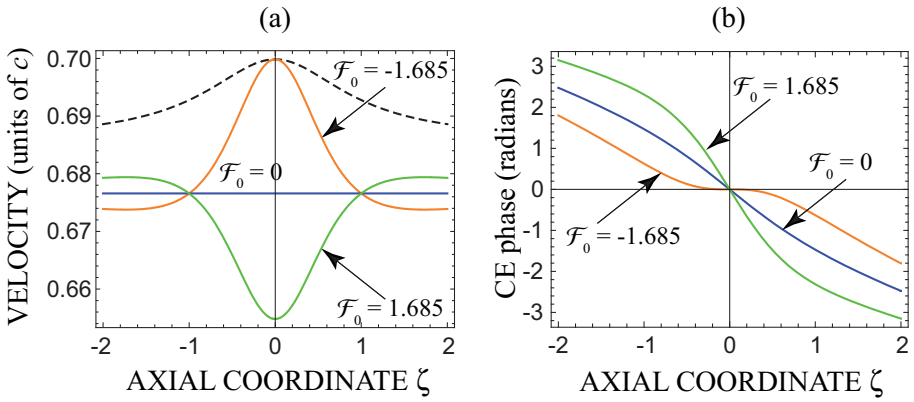

Fig. 3. Phase velocity (dashed line) and group velocity (solid lines) represented in (a) for pulsed Gaussian beams of different $\mathcal{F}_0$ ($\mathcal{L}_0 = 34$) propagating in fused silica at $\omega_0 = 3.14$ fs^{-1}. In (b) we also show the CE phase evolution along the optical axis.

propagating in fused silica. At the mean frequency $\omega_0 = 3.14$ fs^{-1} we have $n_{p0} = 1.458$ and $n_{g0} = 1.478$. As expected, isodiffracting Gaussian beams evidencing an invariant Rayleigh range ($\mathcal{F} = 0$) exhibit a constant group velocity along the optical axis. Of particular importance is the case $\mathcal{F}_0 = -1.685$ for which the phase velocity and the group velocity of the pulsed Gaussian beam matches at the focal point. At the boundaries of the focal volume, $|\zeta| = 1$, a significant mismatch of velocities is clear, which is quantitatively equivalent for different values of $\mathcal{F}_0$.

In order to estimate the CE phase we will not employ Eq. (10) straightforwardly. For convenience we start by considering the fact that

$$\partial_z \varphi(z) = \omega_0 \left(\frac{1}{v_p} - \frac{1}{v_g} \right), \tag{21}$$

which is a magnitude that is accurate at least locally. Therefore, the CE phase of the Gaussian laser beam may be computed as

$$\varphi(\zeta) = \mathcal{L}_0 \int_0^\zeta \left(\frac{c}{v_p} - \frac{c}{v_g} \right) d\zeta = -\arctan(\zeta) - \mathcal{L}_0 \Delta n_0 \zeta - \mathcal{F}_0 \frac{\zeta}{\zeta^2 + 1}, \tag{22}$$

assuming that $\varphi = 0$ at the beam waist. Here $\Delta n = n_g - n$ is the difference of group index and refractive index in the dispersive medium. The CE phase will accumulate the difference shown by the phase shift of the carrier and the phase delay of the wave packet as the pulsed Gaussian beam propagates along the focal region. As a result, the CE phase displays the mismatch growth of the phase and group velocities, as shown in Fig. 3(b). Note that, within the Rayleigh range, the absolute value of the CE phase reaches a minimum for $\mathcal{F}_0 = -1.685$.

3.3 Stationarity of the CE phase

Sensitivity to CE phase is observed for instance in photoionization of atoms (34) and in photoelectron acceleration at metal surfaces mediated by surface plasmon polaritons (35; 36). For those experiments, it may result of convenience to neutralize the CE phase shift of the pulsed laser beam as it propagates in the near field. Stationarity of the CE phase, i.e.

conservation of φ along with the z coordinate, entails a spatiotemporal evolution of the wave field (9) expressed in terms of an spatially-invariant waveform (irrespective of its amplitude). In free space, a rigorous stationary CE phase has been reported solely for X-waves (37). However, finite-energy focal pulses demonstrate a variation of φ upon z due to material dispersion and, importantly, the presence of the Gouy phase. At most, a stationary CE phase may be achieved in a small region around a point of interest, which in our case represents the centre of the waist plane. Thus we reach the stationarity condition $\partial_z \varphi = 0$ at $z = 0$.
From the discussion given above we derive that CE phase stationarity is attained when the phase velocity matches the group velocity in the region of interest. In this case, the spatial-temporal dynamics of the electric field given in (9) in the vicinity of the beam waist may be given in terms of a single variable of the form $t - z/v$. For a pulsed Gaussian beam, the condition of velocity matching at focus, that is $v_p = v_g$ at $\zeta = 0$, is satisfied if

$$\mathcal{F}_0 = -\left(1 + \mathcal{L}_0 \Delta n_0\right). \tag{23}$$

Equivalently Eq. (23) reads $\dot{\mathcal{L}}_0 = -\mathcal{L}_0^2 \Delta n_0 / \omega_0$.
We conclude that CE phase stationarity requires a given spatial dispersion of the wavefield, represented by the parameter $\mathcal{F}$, in order to balance dispersion of the dielectric material Δn_0. In particular, $\Delta n = 0$ in vacuum and therefore $\mathcal{F} = -1$, independently of the beam length. From the numerical simulations shown in Fig. 3 we may also employ the values $n_0 = 1.458$ and $n_{g0} = 1.478$ for fused silica at the frequency $\omega_0 = 3.14$ fs^{-1}, and $\mathcal{L}_0 = 34$ for the pulsed Gaussian beam. In this case Eq. (23) gives $\mathcal{F}_0 = -1.685$. In the vicinity of the beam waist Eq. (22) proves stationarity features at the origin, that is $\partial_\zeta \varphi = 0$, as shown in Fig. 3(b). Moreover, Eq. (23) leads to ultraflattened curves of the CE phase evolution in the focal region since, in fact, $\zeta = 0$ is a saddle point where $\partial_\zeta^2 \phi_0 = 0$.

4. Managing the CE offset

Provided that propagation of ultrashort laser beams is produced with a CE phase commonly running within the Rayleigh range, in this section we analyze a procedure to induce a controlled spatial dispersion leading to keep the CE phase stationary. In particular we exploit dispersive imaging assisted by zone plates to gain control over the waveforms of Gaussian laser beams. Using the *ABCD* matrix formalism, we disclose fundamental attributes of a dispersive beam expander capable of adjusting conveniently the spatial dispersion of the collimated input beam. Some optical arrangements composed of hybrid diffractive-refractive lenses are proposed.

4.1 Focusing pulses with stationary CE phase

We consider a collimated Gaussian beam propagating in vacuum, which has an input Rayleigh range $z_{Rin} = \omega s_{in}^2 / 2c$. This pulsed laser beam impinges over an objective lens in order to produce the required wave field embedded in a dispersive medium of refractive index n_p. The Rayleigh range of the focused field is denoted by z_R. For convenience we assume a nondispersive infinity-corrected microscope objective of focal length f. We also ignore beam truncation. Under the Debye approximation, the width of the Gaussian beam at the back focal plane is (38)

$$s = \frac{2f}{k s_{in}}, \tag{24}$$

provided that $z_R \ll f$. In this model, the focused laser beam is free of focal shifts induced by either a low Fresnel number or longitudinal chromatic aberrations. As a consequence,

the Gaussian lengths of the input ($\mathcal{L}_{in}$) and focused ($\mathcal{L}$) beams satisfies $\mathcal{L}_{in}\mathcal{L} = \omega^2 f^2/c^2 n_p$. Moreover, on-axis dispersion of the fields obeys $\mathcal{F}_{in} + \mathcal{F} = -\Delta n/n_p$.

Equation (23) provides the condition that the focused pulse must fulfil in order to keep its CE phase stationary. This equation leads to a new constraint for the input Gaussian beam. Therefore we recast Eq. (23) showing explicitly the specifications for the input pulse, that yields

$$\mathcal{F}_{in0} = 1 + \frac{\Delta n_0}{n_{p0}} \left(\frac{\omega_0^2 f^2}{c^2 \mathcal{L}_{in0}} - 1 \right). \tag{25}$$

As a consequence, dispersive tailoring of the laser beam reaching $\mathcal{F}_{in0}$ of Eq. (25) leads to CE-phase stationarity near the beam waist of the converging field. Note that if focusing is performed in vacuum, that is assuming $\Delta n_0 = 0$, then $\mathcal{F}_{in} = 1$. In this case the input pulsed field will have a Gaussian width that is independent upon the frequency. In fact, this is a well-established assumption in numerous studies (33).

When focusing is carried out in dispersive bulk media, apparently, Eq. (25) is not generally satisfied by the input laser beam. In principle, modification of $\mathcal{L}_{in0}$ and f by using beam expanders and different microscope objectives, respectively, may result of practical convenience. However, these laser-beam tunings are produced at the cost of resizing the beam spot at the region of interest. This is evident if we express Eq. (25) as $\mathcal{F}_{in0} = 1 + \Delta n_0 \left(\mathcal{L}_0 - n_{p0}^{-1} \right)$. In a majority of applications this is undesirable.

We might conserve typical lengths of inputs and focused beams at ω_0 if, alternatively, spatial dispersion of the laser pulse is altered by modifying $\mathcal{F}_{in0}$. In this case we switch the group velocity of the focused pulse at its waist in order to match a given phase velocity. Next we propose an optical arrangement specifically designed to convert a given collimated pulsed beam, which has a Gaussian length $\tilde{\mathcal{L}}_{in0}$ and a dispersion parameter $\tilde{\mathcal{F}}_{in0}$ that violates Eq. (25), into an ultrashort collimated laser beam of the same length $\mathcal{L}_{in0} = \tilde{\mathcal{L}}_{in0}$ but a different parameter $\mathcal{F}_{in0}$ such that Eq. (25) is satisfied. Thus it conforms a previous step to the focusing action, which will be performed by the microscope objective.

First we may give general features of the required system using the $ABCD$ matrix formalism. A perfect replica (image) of the Gaussian beam is generated if we impose $B = 0$ and $C = 0$, simultaneously. This afocal system provides a lateral magnification $A = D^{-1}$ of the image. Therefore the relationship $z_{Rin} = A^2 \tilde{z}_{Rin}$ is inferred. Moreover, since $\tilde{\mathcal{L}}_{in0} = \mathcal{L}_{in0}$ we derive that $A_0^2 = 1$. In other words, the beam expansion will be unitary at ω_0. Also it may be obtained that

$$\mathcal{F}_{in0} = \tilde{\mathcal{F}}_{in0} + \frac{2\omega_0 \dot{A}_0}{A_0}. \tag{26}$$

As a consequence, dispersion of the matrix element A is required in order to change the spatial dispersion properties of the Gaussian beam, thus switching $\tilde{\mathcal{F}}_{in0}$ for $\mathcal{F}_{in0}$.

The dispersive nature of A also has certain implications with regard to the temporal response of the $ABCD$ system. In particular, the wave field spectrum of the input laser beam will be altered at the output plane of the optical system, since it will be multiplied by the spectral modifier A^{-1}. Under strong corrections carried out at this preprocessing stage, the spectrum of the collimated laser beam might be greatly distorted (39). Ultimately, a spectral shift of the mean (carrier) frequency would be induced, thus urging to recalculate Eq. (25). However, this effect will be neglected in this chapter.

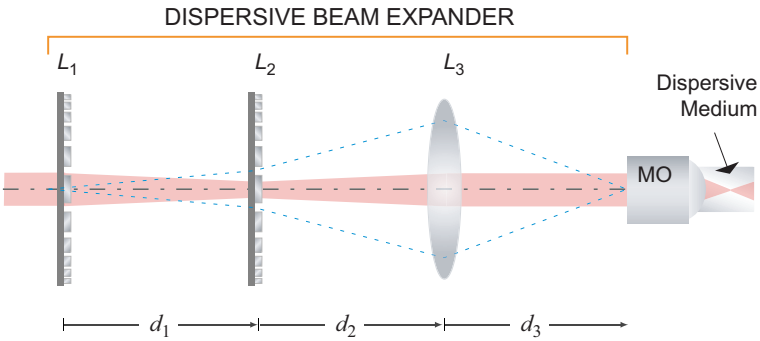

Fig. 4. Schematic diagram of the focusing setup: L_1 and L_2 are components of the diffractive doublet. Also L_3 represents a refractive lens, and MO is the microscope objective.

4.2 Diffraction-induced manipulation of CE dephasing

We propose the thin-lens triplet depicted in Fig. 4 that will perform the necessary spatio-spectral processing of the pulsed Gaussian beam in order to keep stationary its CE shift near the beam waist. This is inspired in the setup shown in (9). Firstly we introduce a doublet composed of kinoform-type zone plates, which are named L_1 and L_2 in Fig. 4, whose dispersive focal lengths are $f_1 = f_{10}\omega/\omega_0$ and $f_2 = f_{20}\omega/\omega_0$. The diffractive doublet is followed by a nondispersive refractive lens (L_3) of focal length $f_3 = f_{30}$. Note that phase-only diffractive lenses may have an optical efficiency of nearly 100% at the carrier frequency ω_0. Neglecting losses induced for instance by material absorption and optical reflections, the kinoform-lens efficiency may be estimated as (40)

$$\eta(\omega) = \mathrm{sinc}^2\left(\frac{\omega}{\omega_0} - 1\right), \tag{27}$$

where $\mathrm{sinc}(x) = \sin(\pi x)/(\pi x)$. We point out that Eq. (27) ignores chromatic dispersion in the lens material to simplify our discussion. This assumption may be given in practice using for instance a diffractive mirror (41). Therefore, the strength of the response η decreases severely at frequencies different of ω_0 due to the appearance of undesirable diffraction orders. This is a relevant effect for subcycle pulses, however it may be negligible for ultrashort beams of sufficiently narrow power spectrum as considered below. Interestingly, diffractive optical elements with high-efficiency responses, which are significantly flatter than η given in Eq. (27) and spanning the visible wavelength range, have been reported in (42) using twisted nematic liquid crystals.

We point out that the $ABCD$ elements of the optical triplet are necessarily dispersive in virtue of the ω-dependent character of f_1 and f_2. The length of the diffractive doublet is d_1, and the coupling distance from L_2 to L_3 is d_2. Furthermore, we assume that L_1 is placed at the waist plane of the input Gaussian beam, whose Rayleigh range is $\tilde{z}_{Rin}$. After propagating through the triplet, the output field is examined at a distance

$$d_3 = \frac{[d_1 d_2 - (d_1 + d_2) f_2] f_3}{d_1(d_2 - f_2 - f_3) + f_2(f_3 - d_2)} \tag{28}$$

from L_3 where the waist image is found ($B = 0$). Therefore the Rayleigh range turns to be $z_{Rin} = -\mathrm{Im}\{q_{in}\}$. For completeness, let us remind the well-known matrix equation for

Gaussian beams

$$q_{in} = \frac{A\tilde{q}_{in} + B}{C\tilde{q}_{in} + D}, \tag{29}$$

being $\tilde{q}_{in} = -i\tilde{z}_{Rin}$ the complex radius of the input laser beam at the plane of L_1.
Distance d_3 given in Eq. (28) depends upon ω. As a consequence, we have control over the waist location of the imaged Gaussian beam for a single frequency. This is of concern when placing the microscope objective. Let us impose d_3 at $\omega = \omega_0$ to be the distance from L_3 to the objective lens (see Fig. 4). The longitudinal chromatic dispersion of the waist plane leads to a dispersive spherical wavefront at the entrance plane of the objective. Ultimately this fact yields a longitudinal chromatic aberration of the broadband focused field. However it may be neglected upon evaluation of the Gaussian Fresnel number $N_G = \mathrm{Re}\{q_{in}\}/z_{Rin}$ (38) of the beam impinging onto the objective lens. Specifically $|N_G| \ll 1$ should be satisfied.
Furthermore, a parametric solution satisfying $B = 0$ and $C = 0$, simultaneously, cannot be found. A sufficient condition may be established by imposing $C_0 = 0$ and $\dot{C}_0 = 0$ so that C vanishes in the vicinity of the carrier frequency. Such a tradeoff is given when

$$f_3 = d_2 + \frac{(d_1 - f_{10})^2}{d_1}, \tag{30}$$

$$f_{20} = -\frac{(d_1 - f_{10})^2}{f_{10}}. \tag{31}$$

This approach suggests that afocality of the the imaging setup is not rigorous but stationary around $\omega = \omega_0$.
Finally, an axial distance $d_2 = f_{10} - d_1$ yields an unitary magnification $A_0 = 1$. Alternatively we may consider that $d_2 = 3f_{10} - d_1 - 2f_{10}^2/d_1$, which gives also a unitary magnification, $A_0 = -1$. In both cases, if additionally

$$f_{10} = d_1 \left(1 + \frac{2}{\Delta\mathcal{F}_{in0}}\right), \tag{32}$$

where the mismatching $\Delta\mathcal{F}_{in0} = \mathcal{F}_{in0} - \tilde{\mathcal{F}}_{in0}$, then it is found that $\dot{A}_0 = A_0\Delta\mathcal{F}_{in0}/2\omega_0$ as requested in (26). We conclude that the focal length of each lens composing the hybrid diffractive-refractive triplet is determined by the parameter $\Delta\mathcal{F}_{in0}$ and the positive axial distance d_1.
Note that $d_2 = f_{10} - d_1$ is positive if $\Delta\mathcal{F}_{in0} > 0$. In the same way $d_2 = 3f_{10} - d_1 - 2f_{10}^2/d_1$ yields a nonnegative real value in the case $\Delta\mathcal{F}_{in0} \leq -4$. As a consequence, our proposal cannot be applied if $-4 < \Delta\mathcal{F}_{in0} \leq 0$ since a negative value of the axial distance d_2 is demanded. In these cases we might consider a different arrangement: a triplet with L_1 being a nondispersive thin lens and L_3 a zone plate instead. Following the analysis given above, it can be proved that a satisfactory dispersive processing is also provided using positive values of d_1 and d_2 in the interval $\Delta\mathcal{F}_{in0} < 0$.
Let us illustrate the validity of our approach by means of a numerical simulation. We consider an isodiffracting Gaussian beam that is focused by a microscope objective lens of $f = 4$ mm. In the image space, the pulsed wave field propagates in fused silica. Note that, from a practical point of view, oil-immersion objectives are suitable to get rid of longitudinal chromatic aberration and focal shifts. An input width $s_{in} = 0.8$ mm ($\mathcal{L}_{in0} = 3.5\ 10^7$) allows that aperturing might be neglected in immersion objectives of NA > 0.75. Numerical computations are performed with the Fresnel-Kirchhoff diffraction formula. At focus we

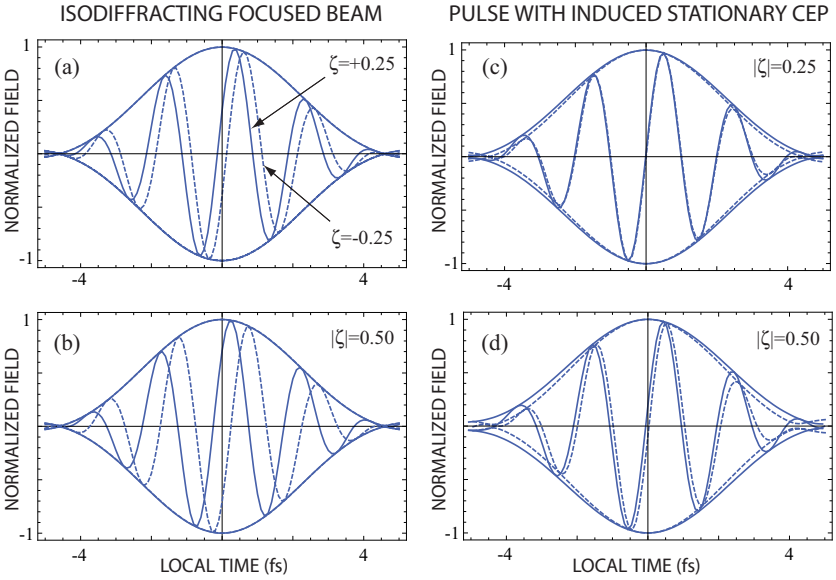

Fig. 5. Evolution of the wave field and envelope at different on-axis points ζ of the focal volume. Negative values of ζ are drawn in dashed lines and positive values in solid lines. Subfigures (a)–(b) correspond to isodiffracting Gaussian beams focused onto bulk fused silica. Time domain is given in terms of the local time t'. In (c)–(d) we employ a procedure to achieve stationarity of the CE phase.

employ a bandlimited signal ε of normalized amplitude spectrum $1 - 2\Omega'^2 + \Omega'^4$ for $|\Omega'| < 1$. Once again, the mean frequency is $\omega_0 = 3.14$ fs^{-1} and the width of the spectral window is $0.8\omega_0$. Figures 5(a) and 5(b) show on-axis waveforms near the focal point. The field envelopes are unaltered in spite of material dispersion. However, the carrier shifts inside the envelope as a reply to the velocity mismatching that it is found at focus, where $v_p = 0.700c$ and $v_g = 0.677c$.

Insertion of the dispersive beam expander of Fig. 4 provides focal waveforms shown in Figs. 5(c) and 5(d). We observe that CE phase is significantly stabilized around the focus, where $\mathcal{L}_0 = 34$ and $\mathcal{F}_0 = -1.685$. In order to minimize the Fresnel number of the pulsed beam to be focused, we have selected $d_1 = 200$ mm leading to a unitary maginfication $A_0 = 1$ and giving $|N_G| < 0.4$ in our spectral window. Equations (30)–(32) yield values for the focal distances of the triplet, $f_{10} = 439$ mm, $f_{20} = -130$ mm, and $f_3 = 525$ mm. We also derive the on-axis distance $d_2 = f_{10} - d_1 = 239$ mm. Importantly, evaluation of Eq. (28) provides a negative axial distance d_3 at the carrier ω_0. This inconvenience is relieved by placing the microscope objective immediately behind L_3 ($d_3 = 0$), as considered in the numerical simulations. This procedure is robust since such an adjustment still maintains the value of v_g switched up to $0.700c$. Inevitably a minor asymmetric pulse broadening is observable. We point out that a relay system might be employed in cases where pulse distortions are dramatic. Placed between the dispersive beam expander and the microscope objective, the relay system may translate the appropriately-corrected virtual pattern of the broadband Gaussian pulse to the entrance plane of the focusing element.

In the numerical simulations, the contribution due to unwanted higher orders of a given kinoform lens is neglected. Considering an input signal S like that observed at focus, the mean efficiency of an ideal diffractive lens may be estimated as

$$\bar{\eta} = \frac{\int_{-1}^{1} |S|^2 \eta d\Omega'}{\int_{-1}^{1} |S|^2 d\Omega'}, \tag{33}$$

which theoretically reaches a value $\bar{\eta} = 0.954$. This fact reveals that higher-order foci carry only 4.6% of the input intensity. Correspondingly, the spectral amplitude shaping the transmitted beam and induced by the thin lenses may be disregarded. Finally, the spectral modifier $\sqrt{\eta}$ altering the input signal S through a kinoform zone plate would also induce a small pulse stretching. As a consequence, the FWHM is estimated to increase from 4.8 fs up to 4.9 fs. Again this phenomenon may be ignored.

5. Conclusions

In summary, we investigated the problem of focusing a few-cycle optical field of Gaussian cross section in order to exhibit a stationary time-domain regime within its depth of focus. For that purpose we established some necessary requirements to be hold by an optical setup to drive pulsed beams with adjustable spatial dispersion. This configuration allows the group velocity of the pulse to be tuned ad libitum keeping the phase velocity unaltered. Therefore dispersive imaging opens the door to fine-tune the electric field of ultrashort laser beams (43; 44). Ultimately the group velocity is regulated at the focal point in order to match the prescribed phase velocity.

We also set forth a dispersive beam expander consisting of a hybrid diffractive-refractive triplet, which is capable of preparing the spatiotemporal response of ultrashort Gaussian pulses to maintain a stationary CE phase along with the optical axis when it is focused within a dispersive medium. Robustness of the optical arrangement is demonstrated upon its coupling with immersion microscope objectives. Finally, the theoretical approach shown in this chapter results promising but still unaccomplished since it must be ratified by experimental evidence.

6. Acknowledgments

This research was funded by the Spanish Ministry of Science and Innovation under the project TEC2009-11635.

7. References

[1] D. J. Jones, S. A. Diddams, J. K. Ranka, A. Stentz, R. S.Windeler, J. L. Hall, and S. T. Cundiff. Carrier-envelope phase control of femtosecond mode-locked lasers and direct optical frequency synthesis. *Science*, 288:635–639, 2000.

[2] G. G. Paulus, F. Lindner, H. Walther, A. Baltuska, E. Goulielmakis, M. Lezius, and F. Krausz. Measurement of the phase of few-cycle laser pulses. *Phys. Rev. Lett.*, 91:253004, 2003.

[3] A. Apolonski, P. Dombi, G.G. Paulus, M. Kakehata, R. Holzwarth, Th. Udem, Ch. Lemell, K. Torizuka, J. Burgdörfer, T.W. Hänsch, and F. Krausz. Observation of light-phase-sensitive photoemission from a metal. *Phys. Rev. Lett.*, 92:073902, 2004.

[4] O. D. Mücke, T. Tritschler, M.Wegener, U. Morgner, F. X. Kärtner, G. Khitrova, and H. M. Gibbs. Carrier-wave rabi flopping: role of the carrier-envelope phase. *Opt. Lett.*, 29:2160–2162, 2004.
[5] A. Baltuska, T. Udem, M. Uiberacker, M. Hentschel, E. Goulielmakis, C. Gohle, R. Holzwarth, V. S. Yakovlev, A. Scrinzi, T.W. Hänsch, and F. Krausz. Attosecond control of electronic processes by intense light fields. *Nature*, 421:611, 2003.
[6] P. Cancio Pastor, G. Giusfredi, P. De Natale, G. Hagel, C. de Mauro, and M. Inguscio. Absolute frequency measurements of the $2^3S_1 \rightarrow 2^3P_{0;1;2}$ atomic helium transitions around 1083 nm. *Phys. Rev. Lett.*, 92:023001, 2004.
[7] M. A. Porras. Diffraction effects in few-cycle optical pulses. *Phys. Rev. E*, 65:026606, 2002.
[8] M. A. Porras, C. J. Zapata-Rodríguez, and I. Gonzalo. Gouy wave modes: undistorted pulse focalization in a dispersive medium. *Opt. Lett.*, 32:3287–3289, 2007.
[9] C. J. Zapata-Rodríguez and M. T. Caballero. Ultrafast beam shaping with high-numerical-aperture microscope objectives. *Opt. Express*, 15:15308–15313, 2007.
[10] C. J. Zapata-Rodríguez and M. T. Caballero. Isotropic compensation of diffraction-driven angular dispersion. *Opt. Lett.*, 32:2472–2474, 2007.
[11] C. J. Zapata-Rodríguez, M. T. Caballero, and J. J. Miret. Angular spectrum of diffracted wave fields with apochromatic correction. *Opt. Lett.*, 33:1753–1755, 2008.
[12] T. E. Sharp and P. J. Wisoff. Analysis of lens and zone plate combinations for achromatic focusing of ultrashort laser pulses. *Appl. Opt.*, 31:2765–2769, 1992.
[13] E. Ibragimov. Focusing of ultrashort laser pulses by the combination of diffractive and refractive elements. *Appl. Opt.*, 34:7280–7285, 1995.
[14] G. M. Morris. Diffraction theory for an achromatic fourier transformation. *Appl. Opt.*, 20:2017–2025, 1981.
[15] G. Mínguez-Vega, E. Tajahuerce, M. Fernández-Alonso, V. Climent, J. Lancis, J. Caraquitena, and P. Andrés. Dispersion-compensated beam-splitting of femtosecond light pulses: Wave optics analysis. *Opt. Express*, 15:278–288, 2007.
[16] P. W. Milonni. *Fast light, slow light and left-handed light*. Institute of Physics Publishing, Bristol, 2005.
[17] L. Xu, Ch. Spielmann, A. Poppe, T. Brabec, F. Krausz, and T. W. Hänsch. Route to phase control of ultrashort light pulses. *Opt. Lett.*, 21:2008–2010, 1996.
[18] Steven T. Cundiff. Phase stabilization of ultrashort optical pulses. *J. Phys. D: Appl. Phys.*, 35:R43–R59, 2002.
[19] R. Ell, J. R. Birge, M. Araghchini, and F. X. Kärtner. Carrier-envelope phase control by a composite plate. *Opt. Express*, 14:5829–5837, 2006.
[20] H. A. Haus and E. P. Ippen. Group velocity of solitons. *Opt. Lett.*, 26:1654–1656, 2001.
[21] Kevin W. Holman, R. Jason Jones, Adela Marian, Steven T. Cundiff, and Jun Ye. Intensity-related dynamics of femtosecond frequency combs. *Opt. Lett.*, 28:851–853, 2003.
[22] Mark J. Ablowitz, Boaz Ilan, and Steven T. Cundiff. Carrier-envelope phase slip of ultrashort dispersion-managed solitons. *Opt. Lett.*, 29:1808–1810, 2004.
[23] A. Rubinowicz. On the anomalous propagation of phase in the focus. *J. Opt. Soc. Am.*, 54:931–936, 1938.
[24] R. W. Boyd. Intuitive explanation of the phase anomaly of focused light beams. *J. Opt. Soc. Am.*, 70:877–880, 1980.
[25] S. Feng and H. G. Winful. Physical origin of the Gouy phase shift. *Opt. Lett.*, 26:485–487, 2001.

[26] Carlos J. Zapata-Rodríguez, David Pastor, and Juan J. Miret. Gouy phase shift in Airy beams. *Opt. Lett.*, (submitted).
[27] L. G. Gouy. Sur une propriété nouvelle des ondes lumineuses. *Compt. Rendue Acad. Sci. (Paris)*, 110:1251–1253, 1890.
[28] Simin Feng, Herbert G. Winful, and Robert W. Hellwarth. Gouy shift and temporal reshaping of focused single-cycle electromagnetic pulses. *Opt. Lett.*, 23:385–387, 1998.
[29] Z. L. Horváth and Zs. Bor. Reshaping of femtosecond pulses by the Gouy phase shift. *Phys. Rev. E*, 60:2337–2346, 1999.
[30] A. B. Ruffin, J. V. Rudd, J. F. Whitaker, S. Feng, and H. G. Winful. Direct observation of the Gouy phase shift with single-cycle Terahertz pulses. *Phys. Rev. Lett.*, 83:3410–3413, 1999.
[31] F. Lindner, G. G. Paulus, H. Walther, A. Baltuška, E. Goulielmakis, M. Lezius, and F. Krausz. Gouy phase shift for few-cycle laser pulses. *Phys. Rev. Lett.*, 92:113001, 2004.
[32] T. Tritschler, K. D. Hof, M. W. Klein, and M. Wegener. Variation of the carrier-envelope phase of few-cycle laser pulses owing to the Gouy phase: a solid-state-based measurement. *Opt. Lett.*, 30:753–755, 2005.
[33] A. E. Siegman. *Lasers*. University Science Books, Mill Valley, 1986.
[34] E. Goulielmakis, M. Uiberacker, R. Kienberger, A. Baltuska, V. Yakovlev, A. Scrinzi, Th. Westerwalbesloh, U. Kleineberg, U. Heinzmann, M. Drescher, and F. Krausz. Direct measurement of light waves. *Science*, 305:1267–1269, 2004.
[35] S. E. Irvine, P. Dombi, Gy. Farkas, and A.Y. Elezzabi. Influence of the carrier-envelope phase of few-cycle pulses on ponderomotive surface-plasmon electron acceleration. *Phys. Rev. Lett.*, 97:146801, 2006.
[36] P. Dombi and P. Rácz. Ultrafast monoenergetic electron source by optical waveform control of surface plasmons. *Opt. Express*, 16:2887–2893, 2008.
[37] M. A. Porras, G. Valiulis, and P. Di Trapani. Unified description of Bessel X waves with cone dispersion and tilted pulses. *Phys. Rev. E*, 68:016613, 2003.
[38] C. J. Zapata-Rodríguez. Debye representation of dispersive focused waves. *J. Opt. Soc. Am. A*, 24:675–686, 2007.
[39] C. J. Zapata-Rodríguez. Focal waveforms with tunable carrier frequency using dispersive aperturing. *Opt. Commun.*, 281:4840–4843, 2008.
[40] V. Moreno, J. F. Román, and J. R. Salgueiro. High efficiency diffractive lenses: Deduction of kinoform profile. *Am. J. Phys.*, 65:556–562, 1997.
[41] J. M. Bendickson, E. N. Glytsis, and T. K. Gaylord. Metallic surface-relief on-axis and off-axis focusing diffractive cylindrical mirrors. *J. Opt. Soc. Am. A*, 16:113–130, 1999.
[42] C. Oh and M. J. Escuti. Achromatic diffraction from polarization gratings with high efficiency. *Opt. Lett.*, 33:2287–2289, 2008.
[43] C. J. Zapata-Rodríguez. Ultrafast diffraction of tightly focused waves with spatiotemporal stabilization. *J. Opt. Soc. Am. B*, 25:1449–1457, 2008.
[44] C. J. Zapata-Rodríguez and M. A. Porras. Controlling the carrier-envelope phase of few-cycle focused laser beams with a dispersive beam expander. *Opt. Express*, 16:22090–22098, 2008.